JVSTA Journal of Vacuum Science & Technology A

Structure in multilayer films of zinc sulfide and copper sulfide via atomic layer deposition

Andrew Short, Leila Jewell, Anthony Bielecki, Trevor Keiber, Frank Bridges, Sue Carter, and Glenn Alers

Citation: Journal of Vacuum Science & Technology A **32**, 01A125 (2014); doi: 10.1116/1.4847956
View online: http://dx.doi.org/10.1116/1.4847956
View Table of Contents: http://scitation.aip.org/content/avs/journal/jvsta/32/1?ver=pdfcov
Published by the AVS: Science & Technology of Materials, Interfaces, and Processing

Structure in multilayer films of zinc sulfide and copper sulfide via atomic layer deposition

Andrew Short, Leila Jewell, Anthony Bielecki, Trevor Keiber, Frank Bridges, Sue Carter, and Glenn Alers[a)]
Department of Physics, University of California at Santa Cruz, 1156 High Street, Santa Cruz, California 95064

(Received 4 September 2013; accepted 30 November 2013; published 18 December 2013)

Multilayer film stacks of ZnS and Cu_xS ($x \sim 2$) were made via atomic layer deposition. The precursors were bis(2,2,6,6-tetramethyl-3,5-heptanedionato)zinc, bis(2,2,6,6-tetramethyl-3,5-heptanedionato)copper, and H_2S generated *in situ* for sulfur. Samples were deposited at 200 °C, in layers ranging from approximately 2 to 20 nm thick, based on binary growth rates. The properties of the film stacks were studied with atomic force microscopy, ultraviolet–visible spectroscopy, and extended x-ray absorption fine structure. The results demonstrate that the structure of films with the thinnest layers is dominated by Cu_xS, whereas in the thicker films, the structure is determined by whichever material is first deposited. This can be attributed to the crystal structure mismatch of ZnS and Cu_xS. © *2014 American Vacuum Society*. [http://dx.doi.org/10.1116/1.4847956]

I. INTRODUCTION

Atomic layer deposition is a well-known technique for the growth of conformal thin films using gas-phase precursors introduced to a substrate separately in half-reaction cycles. Most commonly used for deposition of binary compounds, the atomic layer deposition (ALD) method can also be applied to growing ternary compounds or doped materials.[1–10] ALD operates at relatively low temperatures, allows for deposition into highly structured substrates, and usually allows for direct control of concentration through changing the ratio of number of cycles of each precursor.[11,12] Thus, ALD is an ideal method for creating a thin, highly conformal layer of doped material at low energy cost. However, in the case of ZnS/Cu_xS, the compound material is not as well understood because the structures of ZnS and Cu_xS are incompatible.[13–17] These materials have multiple uses, making this system interesting for study. Thin layers of Cu-doped ZnS powder exhibit low-voltage AC electroluminescence,[18] and these and related materials have fairly small bandgaps. The components are also inexpensive and plentiful, making them potentially attractive for photovoltaics. CuZnS alloys may also be a useful step toward forming the photovoltaic material Cu_2ZnSnS_4.

Often, precursors chosen for ALD are very reactive materials, such as diethylzinc (DEZn).[11,19] These precursors have low boiling points (124 °C for DEZn) and high vapor pressures, which makes them excellent candidates for ALD. However, they are also pyrophoric and difficult to work with (DEZn has a flash point of −18 °C). Therefore, alternative precursors were considered for ALD of ZnS in this work. The precursor chosen for zinc was bis(2,2,6,6-tetramethyl-3,5-heptanedionato)zinc [$Zn(TMHD)_2$], because it is a nonpyrophoric solid precursor used for the chemical vapor deposition of zinc oxide[20] and has been used for ALD of ZnS in previous work.[21] While precursors typically used for the deposition of Cu_2S do not necessarily have the same safety considerations as DEZn [e.g., the low-toxicity, nonflammable $Cu_2(DBA)$],[22] the precursor chosen for copper in this study was Bis(2,2,6,6-tetramethyl-3,5-heptanedionato)copper ($Cu(TMHD)_2$). It has similar safety considerations ($Cu(TMHD)_2$ is nontoxic and nonpyrophoric similarly to $Zn(TMHD)_2$), and also the organic ligands are identical to those of the zinc precursor.

The extended x-ray absorption fine structure technique (EXAFS) was used for much of the analysis of these films. This technique gives information on the local structure about an atom, based on the small oscillations just above its x-ray absorption edge that arise from interference between the outgoing ejected electron wave packet and the backscattered wave from neighboring atoms. An EXAFS analysis is particularly useful for ALD since it is sensitive enough for the small grain sizes produced in low temperatures.[23]

The objectives of this research were to attempt the formation of a copper zinc sulfide alloy on the nanoscale, demonstrate the effect of initial layer growth on a Cu_xS/ZnS nanolaminate structure, and determine if increased layer thicknesses within this structure could stabilize film growth.

II. EXPERIMENT

ALD growth of ZnS and Cu_xS was performed in a custom-built hot wall tube furnace reactor. The base pressure of the system was 20 mTorr. All precursors are introduced into the reactor chamber through separate injectors. Nitrogen was used as the carrier and purge gas at a constant flow rate of 40 sccm. Operating pressure was kept below 2 Torr during pulse and purge cycles.

The precursors used were $Zn(TMHD)_2$ (Strem Chemical, 99% purity), $Cu(TMHD)_2$ (Strem Chemical, 99% purity), and H_2S created *in situ*. $Zn(TMHD)_2$ is a solid powder at room temperature with a melting point of 144 °C and a boiling point of 250 °C at atmospheric pressure. The $Zn(TMHD)_2$ ampoule was heated to 120 °C, and all gas lines were heated to above 90 °C. $Cu(TMHD)_2$ is also a solid powder at room temperature and has a melting point of 198 °C and a boiling point of 315 °C (decomposes) at atmospheric pressure. The ampoule containing $Cu(TMHD)_2$ was heated to 120 °C as well, with the gas lines again maintained above 90 °C. The H_2S was created *in situ* via a reaction between

a)Electronic mail: galers@ucsc.edu

aluminum sulfide powder and water, via the chemical reaction $Al_2S_3 + 3H_2O \rightarrow Al_2O_3 + 3H_2S$. Approximately 2.5 g of Al_2S_3 powder was combined with 30 cc of water for each deposition. After the reaction was completed, the H_2S ampoule was backfilled with N_2, resulting in a partial pressure for H_2S of ~400 mm Hg, and a total pressure in the ampoule equal to ~750 mm Hg. The H_2S gas was passed through a powder desiccant to reduce the residual water content to less than 1% of the H_2S measured with a residual gas analyzer.

If water were present in the hydrogen sulfide there is a concern that ZnO might form instead of ZnS, or Cu_2O might form instead of Cu_2S. However, the reaction $ZnO + H_2S \rightarrow ZnS + H_2O$ is exothermic with an enthalpy of −77 kJ/mol, and $Cu_2O + H_2S \rightarrow Cu_2S + H_2O$ is also exothermic with an enthalpy of −132 kJ/mol.[24] Therefore, any ZnO or Cu_2O that forms *in situ* would be converted to ZnS or Cu_2S, respectively, by the hydrogen sulfide present.

The substrates used were 1 mm thick, 1 in^2 quartz glass microscope slides. The substrates were cleaned via a 30 min sonication in ethanol, and then dried with pressurized nitrogen. Resulting total film thicknesses, morphology, and roughness were measured using an Ambios atomic force microscope in tapping mode. Total thickness was measured by abrasively removing a portion of the film with a razor blade and measuring the step height of the remaining film. Structure was analyzed with EXAFS measurements described in detail below. Bandgaps were determined by ultraviolet–visible spectroscopy (UV–Vis) performed on a StellarNet fiber optic spectrometer.

Using growth behavior observed in previous work for $Zn(TMHD)_2$ (Ref. 21) and in literature for $Cu(TMHD)_2$,[25] a substrate temperature of 200 °C was chosen for this work. The cycle timing sequence chosen was the same as identified in previous work,[21] which is a 25 s purge step, followed by a 5 s H_2S pulse, then another 25 s purge, and finally a 2 s metal precursor pulse (Cu or Zn). With this sequence, alternating layers of ZnS and Cu_xS were grown on quartz substrates.

Four different film layer configurations were studied, which are summarized in Table I. All individual layer thicknesses are estimated from the binary growth rates previously determined,[21] which are equivalent for both materials within the thickness measurement uncertainty. Stack configuration 1a is a "super cycle" of 10 cycles ZnS alternated with 10 cycles Cu_xS. The estimated layer thickness from 10 deposition cycles of either ZnS or Cu_xS is approximately 2 nm. This "super cycle" was repeated 15 times on bare quartz glass, for a total of 150 cycles of each film or 300 cycles total. This also led to stack configurations 1b and 1c, which are the same except with an increased Cu dose time (4 s) for 1c or number of Cu_xS cycles within each "super cycle" (20 cycles instead of 10, still 300 cycles total) for 1b. Stack configuration 1 thus covers thin, layered films with no initial base layer to cause a growth preference. Stack configuration 2 is similar to stack 1a, but in this case, the quartz glass is first coated with a base layer, using 100 cycles of either ZnS or Cu_xS. In this case, the "super cycle" is repeated only 10 times, so the overall film still contains 300 cycles. The 100 cycle base is estimated to be ~20 nm thick. These samples will be considered to have a 2:1 or 1:2 Cu/Zn "target ratio" depending on the base, Cu_xS or ZnS. Stack configuration 2 therefore consists of thin, layered films with a thicker initial base of ZnS or Cu_xS. Stack configuration 3 is a longer "super cycle," alternating 50 cycles of each material (estimated layer thickness of ~10 nm) on quartz glass. In this case, the "super cycle" is repeated only three times, so that the total number of cycles is still 300. These samples will be considered to have a 1:1 Cu/Zn "target ratio." Thus, stack configuration 3 covers thicker, layered films with either ZnS or Cu_xS deposited first. Stack configuration 4 is technically not a stack, but instead 300 cycles of both metal precursors injected simultaneously during the metal precursor step of each cycle. These simultaneous flow films were grown on quartz glass. The total number of cycles for all stack configurations was kept at 300 to keep the expected total film thickness consistent and because of limitations in the amount of H_2S that could be formed at one time.

The EXAFS data were collected at the Stanford Synchrotron Radiation Lightsource on beamline 4-1 using a Si (220) double monochromator, detuned 50% at 9200 eV and 9800 eV for Cu and Zn data, respectively, to reduce

TABLE I. Summary of the four stack configurations used for deposition in this work. The target Cu/Zn ratios are determined by the ratio of Cu/Zn cycles because the deposition rates for the binary compounds are equal within the thickness measurement uncertainty. The measured Cu/Zn ratios are from the relative fluorescent intensities of Cu and Zn during the EXAFS data collection. A "super cycle" refers to the number of Cu:Zn cycles done before repetition, up to the number of "super cycles," except for case 4, where the precursors are dosed simultaneously. In configuration 2, the ZnS base and Cu_xS base are formed from 100 cycles of deposition before any "super cycles" are applied.

	Substrate	"Super cycle"	Number of "super cycles"	Cu:Zn dose time	Target Cu:Zn	Actual Cu:Zn
1 a	Blank quartz	10:10	15	2:2	1:1	1:2
1 b	Blank quartz	20:10	10	2:2	2:1	3:1
1 c	Blank quartz	10:10	15	4:2	2:1	2:1
2	Blank quartz +					
	ZnS base	10:10	10	2:2	1:2	2.2:1
	Cu_xS base	10:10	10	2:2	2:1	3.3:1
3	Blank quartz					
	ZnS 1st	50:50	3	2:2	1:1	1.3:1
	Cu_xS 1st	50:50	3	2:2	1:1	3.9:1
4	Blank quartz	Codeposited	300 cycles	2	1:1	~no Zn

harmonics. The Zn and Cu K-edge data were collected in fluorescence mode with a Ge multichannel detector at a temperature of 8 K. Slit heights were approximately 0.5–0.6 mm, which gives an energy resolution of ~0.9–1.0 eV. The data were reduced using standard techniques (R-space x-ray absorption package),[26] converted to k-space, and Fourier transformed to r-space. The Fourier transform range for all the samples is 3.5–10.5 $Å^{-1}$. The relative concentrations of Zn and Cu were measured by comparison of fluorescence peak heights, to determine a Cu/Zn ratio.

III. RESULTS AND DISCUSSION

A. Photospectroscopy

Optical characterization of the films was performed with ultraviolet–visible spectroscopy (UV–Vis) for determination of the bandgap. ZnS is a direct band gap semiconductor, with a bandgap for films and nanoparticles reported in the literature of 3.5–4.1 eV.[16,17,27–33] Cu_2S has an indirect band gap of 1.2 eV, and a direct band gap of 2.4 eV.[34,35] UV–Vis was performed on films from all stack configurations, and results of configurations 2 and 3 are shown in Figs. 1 and 2. Tauc plots of $(\alpha h\nu)^2$ versus $h\nu$ were used to estimate the direct band gap for the films, and plots of $(\alpha h\nu)^{1/2}$ versus $h\nu$ were used for the indirect bandgap, where α is the absorption coefficient.[36] These films display a direct bandgap between 2.4 and 2.6 eV, matching the expected direct band gap of Cu_2S. In addition, the films examined show an indirect band gap between 1.3 and 1.5 eV, which is close to the accepted value of the indirect Cu_2S band gap. This slightly higher range is hypothesized to be due to the presence of Zn in the films. In these results, no significant differences were observed between films of differing layer thickness or order (stack configuration), or with different Cu/Zn fluorescence ratios (which was above 1 for all films but one in stack configuration 1a).

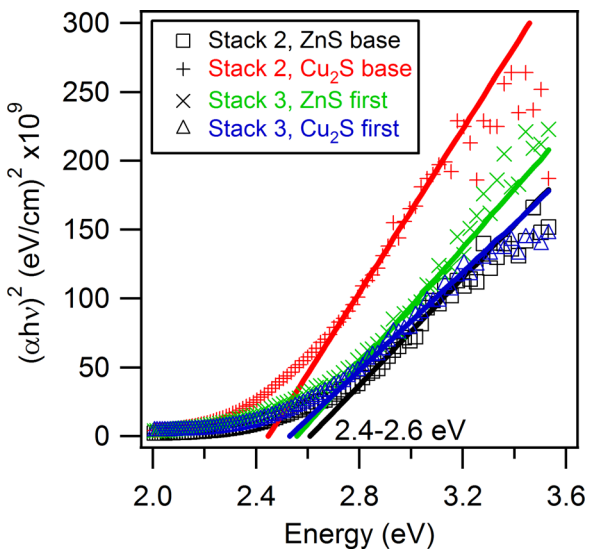

FIG. 1. (Color online) Tauc plot of direct band gap for multilayer alloy CuZnS films in stack configurations 2 and 3. All films have a direct band gap of approximately 2.5 eV, close to the literature direct band gap of Cu_2S.

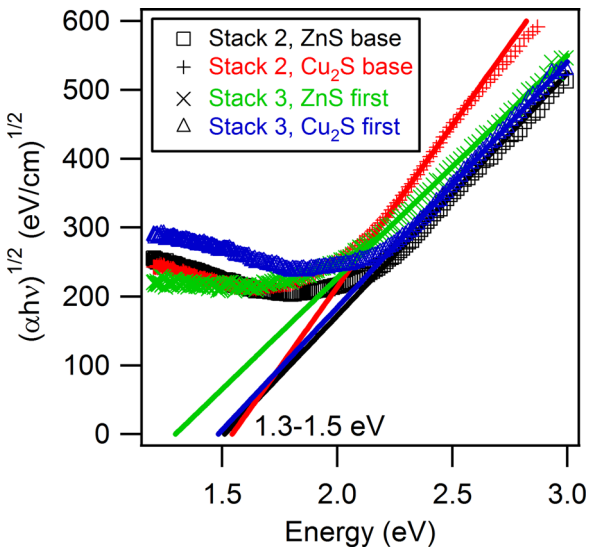

FIG. 2. (Color online) Tauc plot of indirect band gap for multilayer alloy CuZnS films in stack configurations 2 and 3. All films have an indirect band gap between 1.3 and 1.5 eV, slightly higher than the indirect band gap of Cu_2S in literature.

B. Composition and structure via EXAFS

The r-space EXAFS results are plotted in Figs. 3–8 for both the Zn and Cu edges of each sample. These figures plot the real part, R (fast oscillating function), of the fast Fourier transform (FFT) and the envelope, $\pm\sqrt{R^2 + I^2}$, where I is

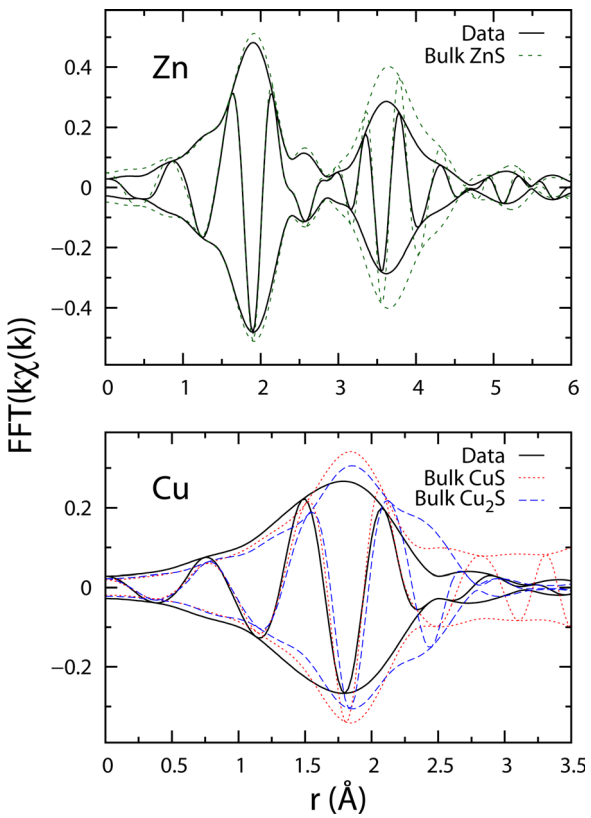

FIG. 3. (Color online) EXAFS r-space plots for films in stack configuration 1a with ZnS deposited first. The result is a thin multilayer film with excess ZnS, where the Zn edge data look very similar to bulk ZnS but the Cu edge plot is disordered.

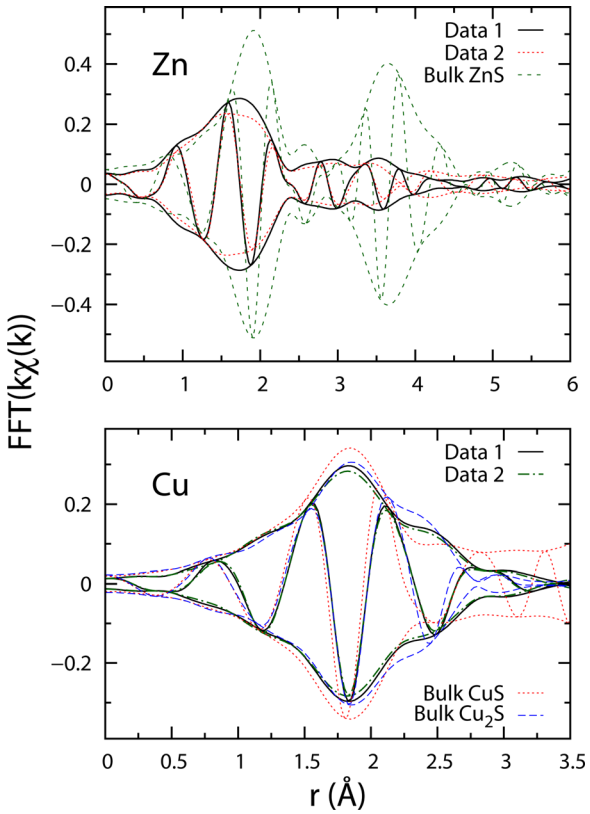

FIG. 4. (Color online) EXAFS results from further attempts at creating ZnS and Cu_xS multilayers, using configurations 1b and 1c. The deposition is nearly the same as before (stack 1a) but the relative Cu precursor dose time (data 1, 1c) or the number of Cu_xS cycles within a "super cycle" (data 2, 1b) are doubled. The environment about Zn is highly disordered and looks more like ZnO, while the Cu edge plot closely resembles bulk Cu_2S.

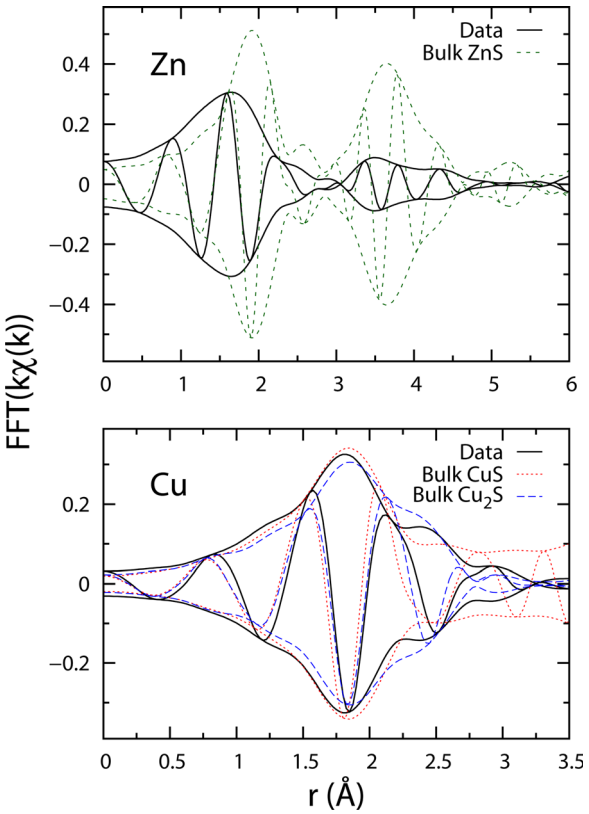

FIG. 5. (Color online) EXAFS r-space plots for films with a ZnS base from stack configuration 2. The overall reduced amplitude in the Zn data indicates increased disorder, while the Cu resembles a linear combination of CuS and Cu_2S. The first peak in the Zn EXAFS looks like Zn-O (see Fig. 10).

the imaginary part of the FFT. For the Zn K edge data, the Zn-S peak is at 1.9 Å, and the second neighbor Zn-Zn peak is near 3.6 Å. For the Cu K edge data, the first peak at 1.8 Å is mainly the Cu-S peak, but the shoulder near 2.0–2.5 Å has a Cu-Cu component. Using the relative fluorescent intensities of Cu and Zn, the ratio of Cu/Zn present in each film was determined during the EXAFS analysis.

For thin multilayers (stack configuration 1a) with parameters for equal depositions of Cu and Zn, the sample contains an unequal Cu/Zn ratio of 1:2. The structure is predominately ZnS, and the Cu_xS fraction is highly disordered, as shown in Fig. 3. The sample might include some ZnS:Cu.

In contrast, for thin multilayers in stack configurations 1b and 1c, the slight excess in Cu deposition pushes the Cu/Zn ratio in the film to 2–3:1. The film is now mostly Cu_2S, and the small Zn fraction is highly disordered ZnS (Fig. 4). Possibly in the latter case, there is a small amount of Zn in Cu_2S.

The measured Cu/Zn fluorescent intensities for stack configurations 2 and 3 were compared with the ratio of Cu/Zn cycles for each respective film stack (see Fig. 9). The cycle ratio includes the 100 cycles comprising the base layer, where present. For example, stack configuration 3 will have a 1:1 cycle ratio of Cu/Zn, while stack configuration 2 with ZnS as the 100 cycle base layer will have a 1:2 cycle ratio of Cu/Zn. It can be seen that the measured Cu/Zn ratio greatly increases for films with a Cu base deposited first, which indicates that ZnS is not deposited as expected in these films. Instead, the first material deposited dominates the structure of the remaining film, and as will be shown below, the increased Cu also correlates with increased Zn surface segregation and oxidation. This may be due to the incompatible structures of Cu_2S and ZnS. ZnS exhibits both cubic and hexagonal structure, including in previous work,[21] but at the unit cell level, the local environment is very similar for both structures. In contrast, Cu_2S and CuS are layered structures—Cu_2S often exists in a monoclinic structure,[13] and CuS is usually a hexagonal phase,[14,15] but quite different from the hexagonal phase of ZnS. In particular, both CuS and Cu_2S structures contain S-S bonds, while the structure of ZnS does not.[16,17] Only when the c-axes of CuS and ZnS align, there is any low-strain crystal structure compatibility.[37]

For a film in configuration 2 with ZnS as the base, the resulting stack surprisingly contains more Cu than Zn. A Cu/Zn ratio of 2.2:1 is observed in the relative fluorescence peaks. For the Zn K edge, the amplitude for the first two peaks is greatly reduced compared to that of bulk ZnS, indicating increased disorder. The first peak is also shifted to lower r (Fig. 5) and is close to the position of Zn-O in ZnO. In addition to the r-shift, another key difference between Zn-S in ZnS and Zn-O in ZnO is the phase of the real part of the Fourier transform, *R*, relative to the envelope, shown in Fig. 10; it can be used as a "fingerprint." Using a linear combination of the theoretical peaks for Zn-O in ZnO and Zn-S

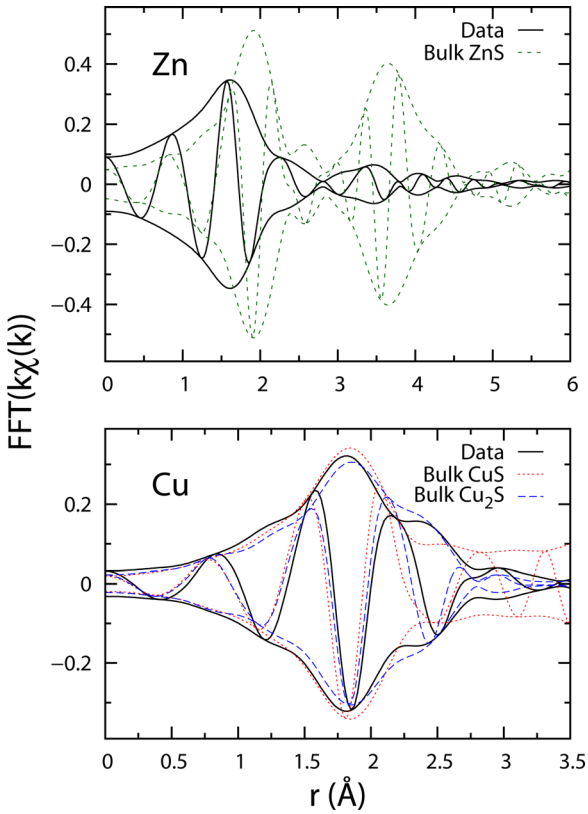

FIG. 6. (Color online) EXAFS r-space plots for films in configuration 2 with a Cu_xS base. Slightly more Cu_2S forms, seen in the increased amplitude of the shoulder ($r \sim 2.3$ Å). The Cu_2S dominates over ZnS formation, with a distorted Zn environment. Again, the first peak in the Zn EXAFS looks like Zn-O (see Fig. 10).

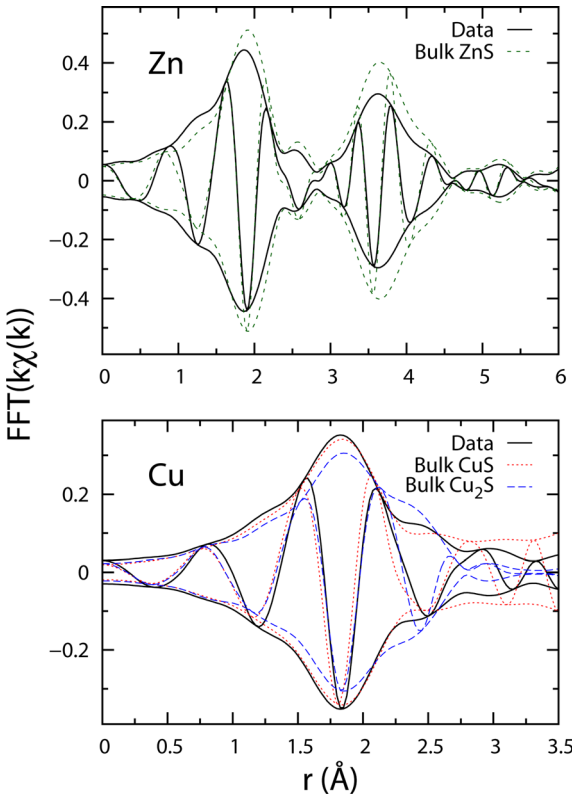

FIG. 7. (Color online) EXAFS r-space plots for films in stack configuration 3 (thicker layers of ZnS and Cu_xS) with ZnS deposited first. The Zn matches bulk results for ZnS, and the Cu contains a combination of CuS and Cu_2S. There are equal amounts of Zn and Cu.

in ZnS, a fit of the data gave the ratio of ZnO:ZnS at roughly 2:1. This indicates that more than half of the ZnS has oxidized to ZnO. Based on the energetics of the oxidation reaction for ZnS ($ZnO + H_2S \rightarrow ZnS + H_2O$ with ΔH about -77 kJ/mol)[24] as well as the lack of any CuO observed, it is unlikely that ZnO is forming during the deposition process; it is also unlikely that the films are oxidizing throughout upon removal from vacuum, since then some CuO would be expected. With these observations, only thin ZnS clumps near the surface will be easily oxidized, making island-like growth of ZnS a likely explanation. Another possibility is that the increased Cu concentration in this film is due to a cation exchange ($ZnS + 2Cu^+ \rightarrow Cu_2S + Zn^{2+}$), as has been seen in this system by Thimsen *et al.*[38] These Zn ions could migrate to the film surface, leading to island-style growth of ZnS. The data for the Cu edge were fit using a linear combination of bulk data for CuS and Cu_2S. In this case, the ratio of CuS:Cu_2S is close to 50/50, with possibly slightly more Cu_2S.

In a stack of configuration 2 with Cu_xS as the base, Cu_xS is favored even more than previously, with a ratio of Cu/Zn of 3.3:1. The Zn edge data (Fig. 6) show a distorted Zn environment in ZnS with an r-shift of -0.16 Å and a change in the phase of the function R, which is again close to Zn-O in ZnO. Based on these shifts and the shape in r-space, most of the Zn is in ZnO. This is confirmed in the fit to a linear

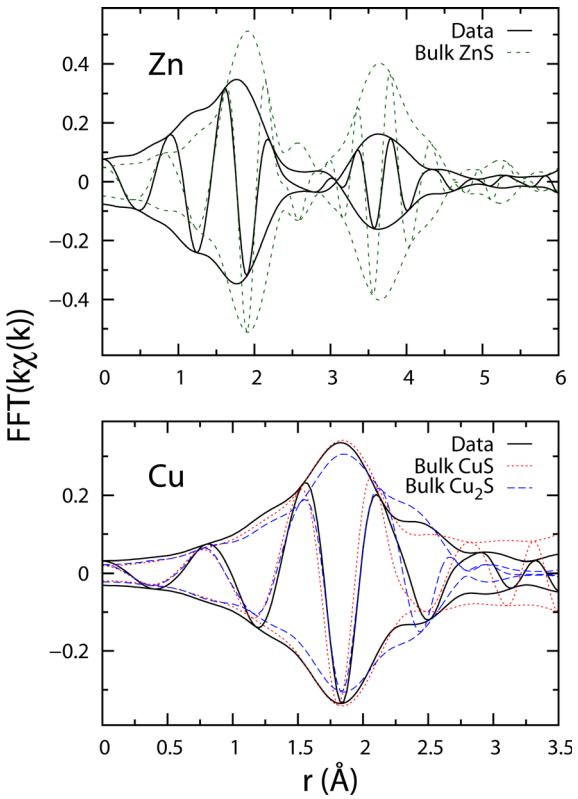

FIG. 8. (Color online) EXAFS r-space plots for films in stack configuration 3 with Cu_xS deposited first. This causes a nucleation delay for ZnS while producing a linear combination of CuS/Cu_2S.

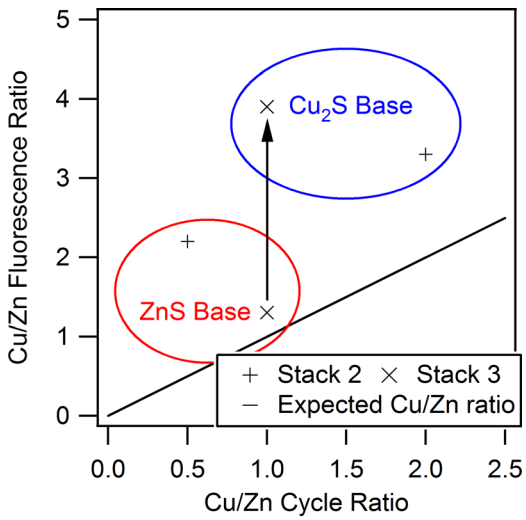

FIG. 9. (Color online) Measured Cu/Zn fluorescence ratio as a function of Cu/Zn cycle ratio for stack configurations 2 and 3. ZnS/Cu_xS base refers to the 100 cycle base for stack configuration 2, or whichever material is deposited first in stack configuration 3. The measured Cu amount dramatically increases for the thick-layered films (configuration 3, 1:1 cycle ratio) when the Cu is deposited first. All films show more copper than expected based on the cycle ratio.

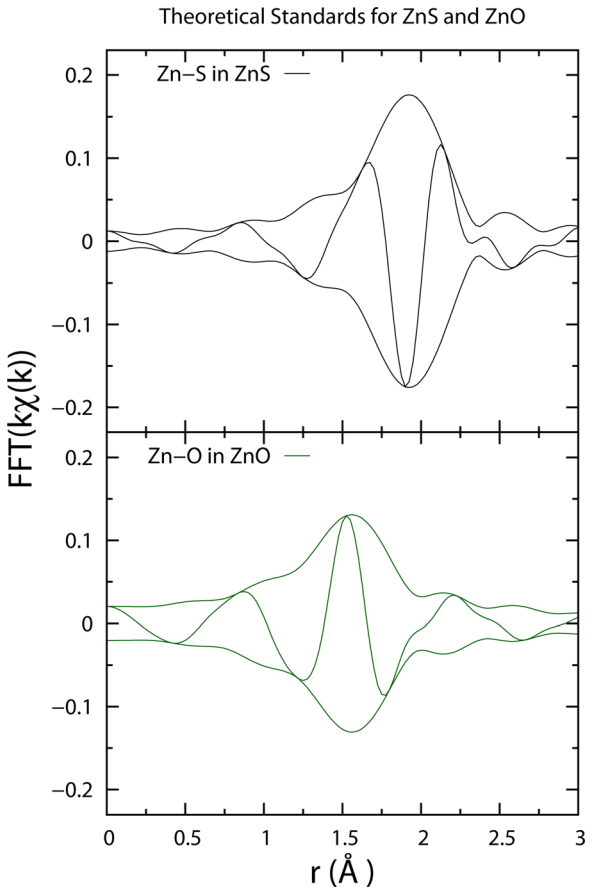

FIG. 10. (Color online) EXAFS theoretical r-space standards of Zn-S in ZnS (top) and Zn-O in ZnO (bottom). The Zn-O peak is shifted to lower r (~1.55 Å) compared to Zn-S (~1.95 Å). The phase of the real part of the Fourier transform of Zn-O is also 180° out of phase relative to the envelope, due to a change in backscattering, compared to the heavier S atom.

combination of ZnO and ZnS, which shows a ZnO:ZnS ratio of 3.2:1.

With thicker layers (~10 nm, stack configuration 3), depositing ZnS first produces nearly equal amounts of Zn and Cu, Cu/Zn = 1.3:1. The Zn K edge data are similar to bulk ZnS (Fig. 7). The overall reduction in amplitude comes from increased disorder in the sample. The sample contains roughly 50/50 CuS:Cu_2S, with slightly more CuS, possibly because the lattices of CuS and ZnS are hexagonal, while the lattice of Cu_2S is monoclinic.[13–17]

Again using configuration 3, but now with Cu_xS first, the resulting multilayer stack contains the largest amount of Cu relative to Zn, with relative Cu/Zn ratio of 3.9:1. The Cu_xS likely causes a nucleation delay for ZnS, as evidenced in the reduced Zn fluorescence peak height and the overall reduced amplitude in the Zn edge EXAFS r-space plot (Fig. 8). The Zn edge data also show a reduction in the second peak height, which means an increase in disorder and possibly smaller grains. Some ZnO is likely present; a fit to the linear combination of ZnO:ZnS yields a ratio of 1:4.3. The Cu edge data for this sample show a 50/50 combination of CuS and Cu_2S, with slightly more CuS. The data fit well to a linear combination of bulk CuS and Cu_2S over a fit range of 1.2–3.8 Å; however, the fit matches the data well out to 6 Å (not shown). This confirms that a linear combination model describes the data well.

The codeposited samples (configuration 4) also highly favor Cu, with approximately no Zn and mostly Cu_xS in the sample. The samples contain more CuS than Cu_2S (~85/15), and this ratio is independent of the fit range. There is too little Zn in either case to obtain sufficiently good EXAFS data to do a detailed analysis; the Zn structure is disordered and again looks more like Zn-O.

C. Surface roughness of ALD multilayers

Film roughness was studied for the 10 nm thick multilayer films (stack configuration 3) and for the 2 nm thick layered films on 20 nm ZnS and Cu_xS base layers (stack configuration 2). The RMS roughness as determined by AFM as well as the percent roughness is plotted in Fig. 11 as a function of

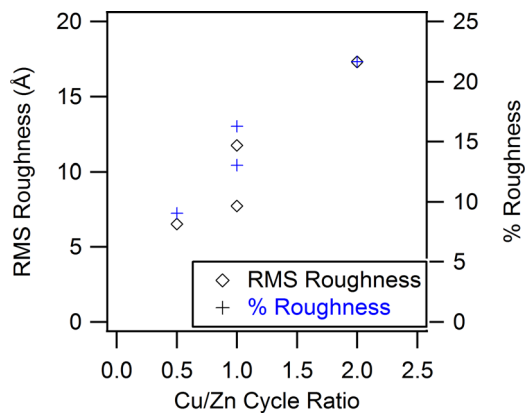

FIG. 11. (Color online) Plot of roughness and % roughness as a function of Cu/Zn cycle ratio for films from stack configurations 2 and 3. There is a clear trend of increasing film roughness with more copper precursor cycles.

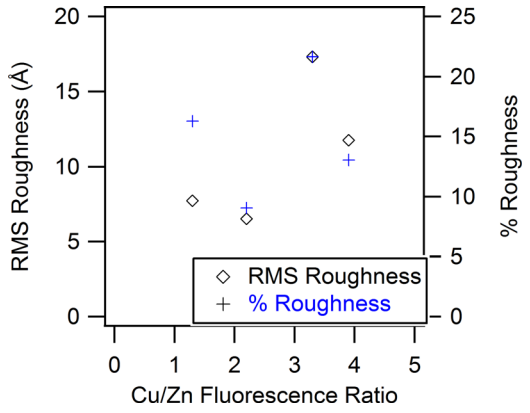

FIG. 12. (Color online) RMS roughness and % roughness vs measured Cu/Zn fluorescence ratio for films in stack configurations 2 and 3. There is a general trend of increased roughness with increased Cu content.

Cu_xS/ZnS cycle ratio. It can be seen that the roughness increases with more Cu cycles, causing the percent roughness to vary from 9% to 22%. The RMS and percent roughness from AFM is also plotted as a function of the Cu/Zn ratio (measured by fluorescence intensity on the EXAFS setup) in Fig. 12. While the roughness as a function of measured Cu content is not correlated as clearly, this may be attributed to uncertainty in the measured Cu/Zn ratio. This increase in roughness with Cu content/cycles may indicate that Cu grows as islands, or in a preferred orientation.

Film roughness also generally increases with ZnO content, when ZnO is observed, as shown in Fig. 13. The AFM percent roughness is plotted as a function of the percent ZnO content, which is determined by the EXAFS fit to ZnS/ZnO; again the Cu/Zn ratio is from the ratio of the Cu and Zn fluorescence. This suggests that when the film is mostly Cu_xS, the small amount of Zn is pushed to the surface in small islands that are easily oxidized.

Interestingly, in the films with simultaneous precursor flow (stack configuration 4), the percent roughness is only 5.3%, with almost no included ZnS (almost no Zn fluorescence in EXAFS). Although the Zn is not included in the films, it may be stabilizing the growth of the Cu_xS during the precursor dosing step or limiting the amount of ZnO present, as the percent roughness is lower than in other films.

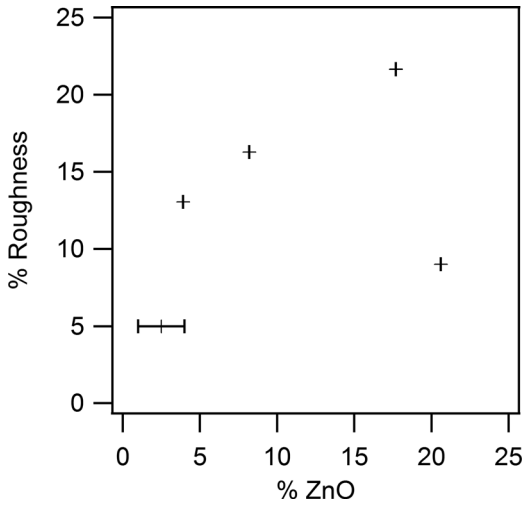

FIG. 13. Percent roughness as a function of percent ZnO content. With one exception, the roughness increases as the % of ZnO increases. The large error bars on the lowest % ZnO value are due to low Zn EXAFS signal.

IV. SUMMARY AND CONCLUSIONS

ALD of ZnS/Cu_xS multilayer/alloy stacks using $Zn(TMHD)_2$, $Cu(TMHD)_2$, and *in situ* generated H_2S has been demonstrated. The indirect band gap obtained from Tauc plots was 1.3–1.5 eV, slightly higher than the literature value for Cu_2S. The band gap may be from the films containing mostly Cu, with the slightly higher band gap than the bulk Cu_2S value due to the Zn additions. The EXAFS data also indicate that when the Cu/Zn ratio is high, Zn is entering the multilayer films in a highly disordered, nearly amorphous state; possibly some of the Zn is doping a primarily Cu_xS film. In some cases, ZnS oxidation occurs after the deposition, based on the lack of CuO present, which suggests that the oxidized ZnS is primarily on the surface where it is unprotected. The surface roughness increases with Cu content, indicating perhaps an island or oriented growth mechanism for Cu_xS and ZnS in these multilayered structures.

ACKNOWLEDGMENTS

This work was supported by National Science Foundation grant DMR-1006190. The EXAFS experiments were carried out at the Stanford Synchrotron Radiation Light source, operated by the DOE, Division of Chemical Sciences.

[1]V. Mikkulainen, M. Leskela, M. Ritala, and R. L. Puurunen, J. Appl. Phys. **113**, 021301 (2013).
[2]L. Karvonen *et al.*, Appl. Phys. Lett. **103**, 031903 (2013).
[3]Y. Z. Gu, H. L. Lu, Y. Geng, Z. Y. Ye, Y. Zhang, Q. Q. Sun, S. J. Ding, and D. W. Zhang, Nanoscale Res. Lett. **8**, 107 (2013).
[4]D. Martin, M. Grube, W. Weinreich, J. Muller, W. M. Weber, U. Schroder, H. Riechert, and T. Mikolajick, J. Appl. Phys. **113**, 194103 (2013).
[5]H. Seim, H. Mölsä, M. Nieminen, H. Fjellvåg, and L. Niinistö, J. Mater. Chem. **7**, 449 (1997).
[6]J. H. Song, E. D. Sim, K. S. Baek, and S. K. Chang, J. Cryst. Growth **214**, 460 (2000).
[7]E. B. Yousfi, B. Weinberger, F. Donsanti, P. Cowache, and D. Lincot, Thin Solid Films **387**, 29 (2001).
[8]M. Juppo, P. Alén, M. Ritala, and M. Leskelä, Chem. Vapor Depos. **7**, 211 (2001).
[9]J. W. Elam, Z. A. Sechrist, and S. M. George, Thin Solid Films **414**, 43 (2002).
[10]J. W. Elam and S. M. George, Chem. Mater. **15**, 1020 (2003).
[11]S. M. George, Chem. Rev. **110**, 111 (2010).
[12]T. Suntola and J. Hyvarinen, Annu. Rev. Mater. Sci. **15**, 177 (1985).
[13]H. T. Evans, Science **203**, 356 (1979).
[14]W. Liang and M. H. Whangbo, Solid State Commun. **85**, 405 (1993).
[15]S. W. Goh, A. N. Buckley, and R. N. Lamb, Miner. Eng. **19**, 204 (2006).
[16]K. S. Rathore, D. Patidara, Y. Janu, N. S. Saxena, K. Sharma, and T. P. Sharma, Chalcogenide Lett. **5**, 105 (2008).
[17]Y. S. Kim and S. J. Yun, Appl. Surf. Sci. **229**, 105 (2004).
[18]S. Medling, F. Bridges, and S. A. Carter, J. Lumin. **134**, 251 (2013).
[19]J. T. Tanskanen, J. R. Bakke, T. A. Pakkanen, and S. F. Bent, J. Vac. Sci. Technol. A **29**, 031507 (2011).
[20]L. V. Saraf, M. H. Engelhard, C. M. Wang, A. S. Lea, D. E. McCready, V. Shutthanandan, D. R. Baer, and S. A. Chambers, J. Mater. Res. **22**, 1230 (2007).
[21]A. Short, L. Jewell, S. Doshay, C. Church, T. Keiber, F. Bridges, S. Carter, and G. Alers, J. Vac. Sci. Technol. A **31**, 01A138 (2013).
[22]A. B. F. Martinson, J. W. Elam, and M. J. Pellin, Appl. Phys. Lett. **94**, 123107 (2009).

[23]F. Jiménez-Villacorta, A. Muñoz-Martín, and C. Prieto, J. Appl. Phys. **96**, 6224 (2004).
[24]D. D. Wagman, W. H. Evans, V. B. Parker, R. H. Schumm, and I. Halow, *The NBS Tables of Chemical Thermodynamic Properties* (National Standard Reference Data System, 1982), pp. 38, 57, 138, 139, 154, 155.
[25]L. Reijnen, B. Meester, F. de Lange, J. Schoonman, and A. Goossens, Chem. Mater. **17**, 2724 (2005).
[26]C. H. Booth, "R-space x-ray absorption package" (2010). See: http://lise.lbl.gov/RSXAP/.
[27]R. G. Zhang, B. Y. Wang, and L. Wei, Vacuum **82**, 1208 (2008).
[28]P. Prathap, N. Revathi, Y. P. V. Subbaiah, and K. T. R. Reddy, J. Phys.-Condens. Mater. **20**, 035205 (2008).
[29]K. R. Murali, S. Vasantha, and K. Rajamma, Mater. Lett. **62**, 1823 (2008).
[30]Q. Liu and G. B. Mao, Surf. Rev. Lett. **16**, 469 (2009).
[31]F. Gode, C. Gumus, and M. Zor, J. Cryst. Growth **299**, 136 (2007).
[32]K. Sreejith, K. S. Mali, and C. G. S. Pillai, Mater. Lett. **62**, 95 (2008).
[33]J. P. Borah and K. C. Sarma, Acta Phys. Pol. A **114**, 713 (2008).
[34]R. Marshall and S. S. Mitra, J. Appl. Phys. **36**, 3882 (1965).
[35]I. Grozdanov and M. Najdoski, J. Solid State Chem. **114**, 469 (1995).
[36]J. Tauc, Mater. Res. Bull. **3**, 37 (1968).
[37]S. Medling, C. France, B. Balaban, M. Kozina, Y. Jiang, F. Bridges, and S. A. Carter, J. Phys. D: Appl. Phys. **44**, 205402 (2011)
[38]E. Thimsen, Q. Peng, A. B. Martinson, M. J. Pellin, and J. W. Elam, Chem. Mater. **23**, 4411 (2011).